The influence of the film thickness of nanostructured α-Fe_2O_3 on water photooxidation

Flavio Leandro Souza, Kirian Pimenta Lopes, Elson Longo and Edson Roberto Leite*

Received 14th July 2008, Accepted 12th November 2008
First published as an Advance Article on the web 8th January 2009
DOI: 10.1039/b811946e

The present work shows the influence of the film thickness in the optical and photoelectrochemical properties of nanostructured α-Fe_2O_3 thin film. We found that the film thickness has a strong influence on the optical absorption and the results here reported can help in the design of nanostructured α-Fe_2O_3 with superior performance for water photo-oxidation. The results show that the optical property of the hematite film is affected by the film thickness, probably due to the stress induced by the strong interaction between film and substrate. This stress generates defects in the crystal lattice of the hematite film, increasing the (e^-)–(h^+) recombination process.

Introduction

Based on Fujishima and Honda's[1] pioneering work, world-wide research has focused on the conversion of sunlight into hydrogen as a clean and renewable energy source. In the classical work, the authors showed that it is possible to induce the water-splitting by light, using TiO_2 semiconductor as photoanode. However, TiO_2 has a wide band gap and is hence photoexcited by UV light only (which occupies 5% of the solar spectrum). The main focus of the present research is to shift the activity of the photoanode into the visible region of the sunlight, aiming to increase the energy conversion efficiency.[2–4] The iron oxide (α-Fe_2O_3 or hematite) is a semiconductor material with a narrow band gap (approximately 2.2 eV) and very good electrochemical stability in water. These properties make this material especially attractive when used as a photoanode to split the water into oxygen and hydrogen by sunlight. Theoretical calculations[5] suggest that this semiconductor presents a maximum efficiency of 12.9%, however the reported water splitting efficiency for α-Fe_2O_3 is much lower.[6–9] Actually, we can attribute several reasons to this discrepancy, such as: small optical absorption coefficient, rapid electron(e^-)-hole(h^+) recombination resulting in short carrier diffusion lengths (in the range of 2–4 nm,[10] 20 nm[11]) and slow surface reaction kinetics.

An approach to improve the conversion efficiency is the development of nanostructured α-Fe_2O_3 thin films.[8,12] The introduction of the nanometric scale can improve the surface reaction kinetics (due to the increase of interfacial reaction area) and avoid the electron–hole recombination due to the short diffusion path of the hole up to the surface in a nanostructured material (with crystal size close to the diffusion length of the hole). This approach seems to be very attractive, however the influence of the nanoscale structure in the optical absorption of α-Fe_2O_3 is not well known. In this work, we report the influence of the film thickness in the optical and photoelectrochemical properties of nanostructured α-Fe_2O_3 thin film. We have found that the film thickness has a strong influence on the optical absorption and the results here reported can help in the design of nanostructured α-Fe_2O_3 with superior performance for water photo-oxidation. In this study, the hematite film was doped with Si (0.5% wt). This silicon concentration demonstrated the best photocurrent performance, compared to the pure hematite or to hematite doped with higher Si concentration.

Experimental

The hematite thin film was prepared by spin coating solution deposition of a polymerisable precursor. This method was used in our research group to process several kinds of metal oxide thin films and was selected as it enabled to obtain nanostructured films with good stoichiometric and thickness control.[13] The process is based on the synthesis of a soluble polymeric precursor with the metals arrested in the polymeric chain. A hydrocarboxylic acid, such as citric acid, is used to chelate the ions of interest. Following this step, the addition of a glycol such as ethylene glycol leads to the formation of a soluble polyester. The polymerization processes, promoted by heating the mixture, result in a homogeneous polymer in which metal ions are uniformly distributed throughout the organic matrix. In a typical synthesis procedure, citric acid ($[C_6H_8O_7]$) was dissolved in anhydrous ethyl alcohol and heated to a temperature of 60 °C. Then, iron(III) nitrate ($[Fe(NO_3)_3{\cdot}9H_2O]$) and tetra-ethyl-*orto*-silicate (TEOS–$Si(CH_2CH_2OH)_4$) was mixed into the citric acid solution under constant stirring in a molar ratio of 3 : 1 ([citric acid]/[Fe + Si]). After homogenization of the solution containing Fe + (0.5%wt)Si, ethylene glycol ($C_2H_6O_2$) was added to the mixture in a citric acid/ethylene glycol ratio of 60 : 40 wt%. The resulting solution was stirred and heated

LIEC-CDMDC—Department of Chemistry, UFSCar, São Carlos, SP, Rodovia Washington Luiz, km 235, C.P. 676, CEP 13565-905 São Carlos, SP, Brazil. E-mail: derl@power.ufscar.br; Fax: +55 16 3361-5215; Tel: +55 16 33518214

until it reached citrate polymerization by the polyesterification reaction. In this step, a high viscosity liquid is obtained. After the polymerization step, the viscosity was adjusted (decreased) by the addition of ethyl alcohol. The solution was deposited onto a transparent conducting glass substrate (FTO- fluorine doped SnO_2 $R_\Omega < 15\ \Omega\ cm^{-1}$), where spin coating was conducted at a rotation speed of 7000 rpm. After deposition, the substrate was heated on a hot plate at 50 °C for the solvent evaporation and heat treated at 500 °C for 2 h for the film crystallization (heating and cooling rate of 1 °C min^{-1}). In order to control the film thickness, the solution viscosity was adjusted as well as the number of deposition layers. For instance, to obtain a film of 165 nm, four layers were deposited (with complete deposition cycle, *i.e.*, deposition and heat treatment).

The film morphology and thickness (by cross section analysis of the cleaved sample) were characterized by FE-SEM (Zeiss Supra 35). The crystalline phases were identified by XRD (Rigaku D-Max 200, using Cu Kα radiation) and the optical characterization of the film was performed using a Cary 5E UV-Vis spectrophotometer. The photoelectrochemical measurements were carried out in a standard three-electrode cell using the hematite film as the working electrode (1.5 cm^2 area), Ag/AgCl in KCl saturated solution as reference electrode and platinum wire as counter electrode. A 1.0 M NaOH (Merk pro-analysis in high pure water, pH = 14) solution was used as the electrolyte. A scanning potentiostat (Potentiostat/Galvanostat μAutolab III) was used to measure dark and illumination current at a scan rate of 50 mV s^{-1}. Sunlight (1000 W m^{-2}) was simulated with a 450 W xenon lamp (Osram, ozone free) and AM1.5 filter. The light intensity was set at 100 mW cm^{-2}. The incident photo-to-current conversion efficiency (IPCE) was measured as a function of the excitation wavelength (λ) using a 300 Xe lamp coupled to a Jobin–Ivon monochromator (typical light intensity of 940 μW cm^{-2} at 500 nm). The IPCE was calculated considering the following equation:[4] IPCE = 1240(eV nm). Photocurrent density (μA cm^{-2})/[λ(nm). Irradiance (μW cm^{-2})].

Results and discussion

The deposition method used in this work produced orange–red transparent films with four different thicknesses (25, 66, 85 and 165 nm). Fig. 1 illustrates the cross section and the top-view analysis of the films morphology characterized by field emission scanning electron microscopy (FE-SEM). The thinner film (Fig. 1a and b) showed a thickness of 25 nm with a uniform and continuous morphology. The top view analysis exhibits the nanostructured nature of the film, with elongated grains and diameter ranging from 20–30 nm and length of 60–100 nm. The analysis suggests that this film is formed by a single hematite grain layer. The thicker film (Fig. 1c and d) showed a thickness of 165 nm with a top view morphology quite similar to the thinner film. However the cross section analysis suggests that the film is formed by several grain layers. This cross section morphology is typical of films prepared by solution deposition and multiple deposition steps. X-Ray diffraction (XRD) pattern of the films with different thicknesses, shown in Fig. 2, exhibits the formation of hematite

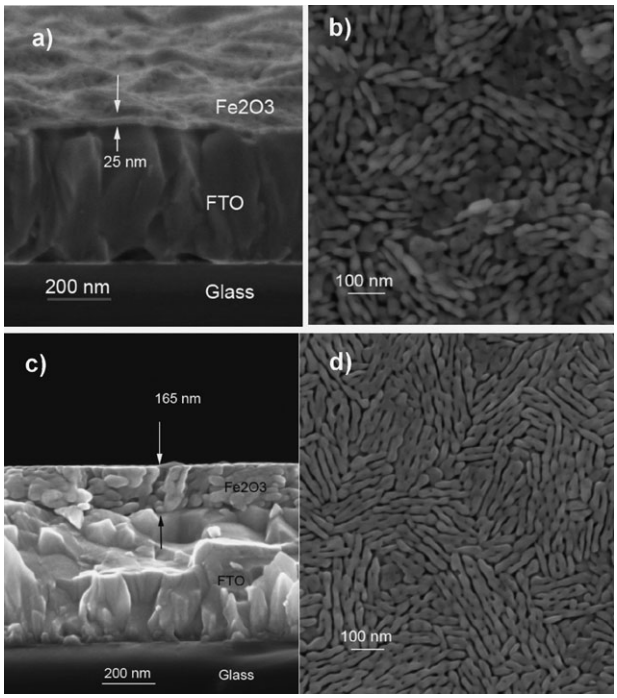

Fig. 1 Cross section and top-view analysis of the films morphology characterized by secondary electron (using an in-lens detector) in a FE-SEM: (a) cross section of the thinner film (25 nm); (b) top-view of the thinner film (25 nm); (c) cross section of the thicker film (165 nm); (d) top-view of the thicker film (165 nm).

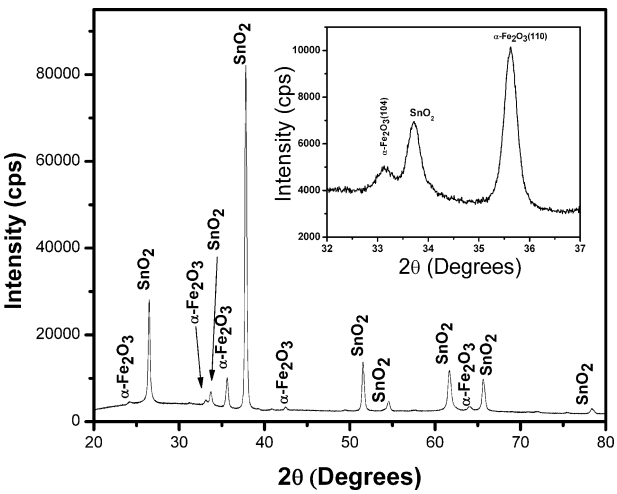

Fig. 2 XRD pattern of the film (165 nm thickness). The inset shows details of the hematite phase with preferential orientation in the [110] axis vertical to the substrate.

phase with preferential orientation in the [110] axis vertical to the substrate (see inset of Fig. 1), even for the thinner film. This result indicates that the (001) plane is oriented vertically to the substrate. It is well know that the hematite presents a strong anisotropy in electronic conductivity. Actually the conductivity in the basal plane (001) is up to 4 orders of magnitude higher than the orthogonal planes[8] and this preferential orientation should facilitate the collection of electrons during the photooxidation process. A similar orientation

was observed by several authors[6–9] using different deposition methods. The crystallite size for the thicker film (165 nm), calculated from XRD data and Scherrer's equation considering the (110) and (300) planes, were 54 and 27 nm, respectively, indicating the presence of elongated crystalline domains and corroborating with the FE-SEM analysis. The films with intermediate thickness (66 and 85 nm) showed very similar morphology and structure.

Fig. 3 shows the current–potential curves of the films with different thicknesses under illumination. It is important to point out that the dark current is negligible up to 0.6 V. We can observe that the photocurrent at 0.23 V (corresponding to 1.23 V_{RHE}) increases with increasing film thickness. At 0.23 V the photocurrent density of the 165 nm thick films is 3.4×10^{-5} A cm^{-2} and at 0.6 V, the thicker film presents a photocurrent density of 1.5×10^{-4} A cm^{-2}. It is interesting to observe a dependence of the photocurrent density on the film thickness, *i.e.*, the photocurrent density decreases with decreasing film thickness. When we look at the absorption coefficient (α) as a function of the wavelength, shown in Fig. 4, and calculated from the optical absorption data and the film thickness, we observe that the thinner film (25 nm) presents the highest α value in the entire wavelength analyzed, when compared to the thicker films (of 66, 85 and 165 nm). How can we explain the low photocurrent density, given that the thin 25 nm thick film presented the highest α and should present the smallest diffusion length for the h^+ to reach the surface? In order to answer this question we performed the IPCE measurement of the 25 nm and 85 nm thick film in two different potentials (at 0.23 and 0.60 V). Fig. 5a shows the IPCE curves measured at a potential of 0.23 V and it can be observed that the thinner film presented a very low IPCE value in relation to the thicker film. It can be observed that both films presented the highest IPCE value in a low wavelength (around 300 nm). When we increase the potential to 0.60 V (Fig. 5b), the IPCE value increases and both films present very similar values in the entire wavelength measured. These results clearly suggest that the (e^-)–(h^+) recombination process in the

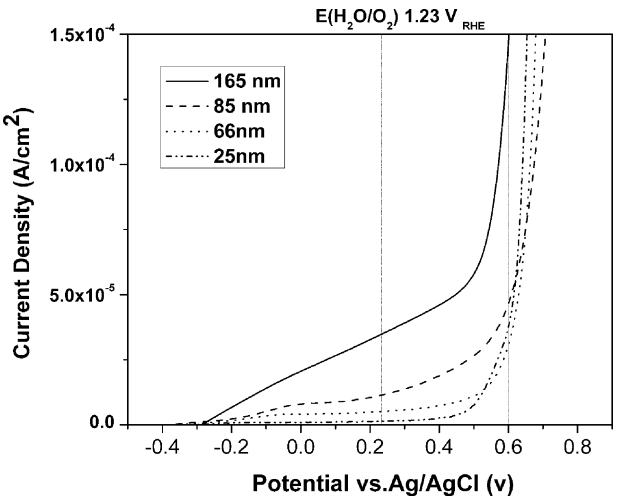

Fig. 3 Current–potential curves of the films with different thicknesses under illumination. The light intensity was set at 100 mW cm^{-2}.

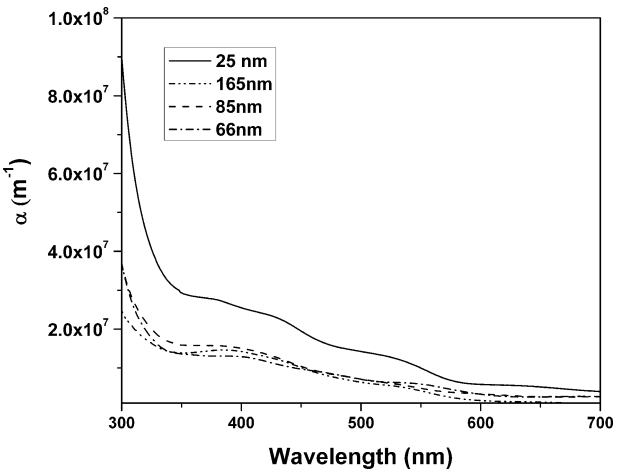

Fig. 4 Absorption coefficient (α) as a function of the wavelength for the hematite films with different thicknesses.

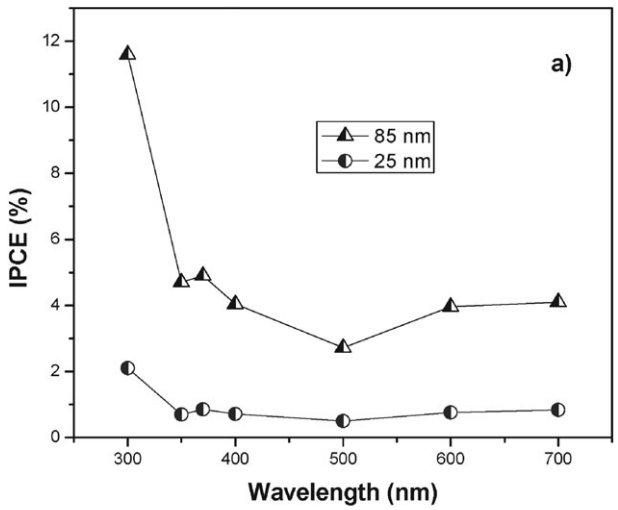

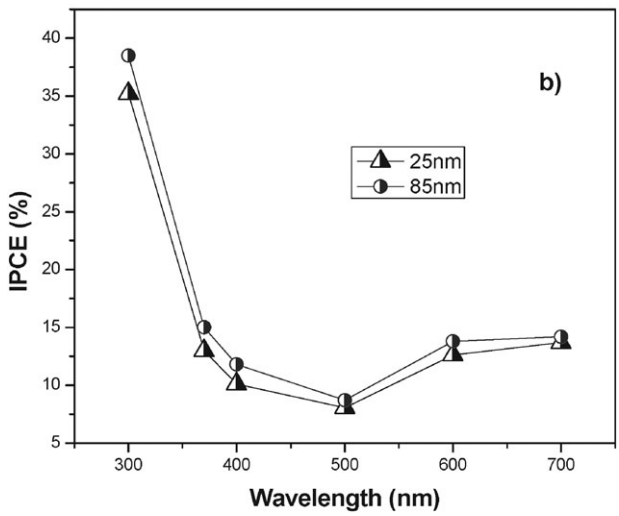

Fig. 5 (a) IPCE curves measured at a potential of 0.23 V for the film with a thickness of 25 and 85 nm; (b) IPCE curves measured at a potential of 0.60 V for the film with a thickness of 25 and 85 nm.

thinner film is high. Such holes can reach the surface by diffusion only if their recombination with electrons is prevented by a stronger electron depletion achieved at more positive polarization (at a higher potential).

Now, a new question arises. Why does the thinner film present a higher (e^-)–(h^+) recombination process? In order to answer this question, we estimated the nature and onset of the electronic transitions of the films with thicknesses of 25 and 165 nm. These estimations were performed considering the following equation:[14]

$$(\alpha\, h\nu) = A_o(h\nu - E_g)^m \qquad (1)$$

where $h\nu$ is the photon energy (in eV), E_g is the optical band gap energy (in eV) and A_o and m are constant, which depend on the kind of electronic transition, where m is equal to 1/2 for a direct allowed and 2 for an indirect forbidden transition. Fig. 6a and b show the plot of absorption data according to eqn (1). We can observe that the 25 and 165 nm thick films present an indirect band gap energy of 1.76 and 1.83 eV, respectively (Fig. 6a). Considering the direct band gap energy (Fig. 6a), a significant difference between both films is observed. The thicker film presented a single transition of 2.7 eV while the thinner film presented three transitions, indicating the presence of intermediate energy levels. Further experimental and theoretical investigations are needed to draw a clear picture of the energy band gap–structure and transitions for different film thicknesses. These intermediate energy levels observed in the thinner film must be related to trapped electrons close to the conduction band. The origin of these intermediate levels is not clear yet; however we believe that it must be associated to the stress induced by the strong interaction between the film and the substrate. This effect is not observed in the thicker film due to the stress relaxation induced by deposition of several hematite layers performed during the film preparation. It is important to point out that the presence of these intermediate levels can also explain the highest α value measured for the thinner film. Based on the optical band gap energy analysis, we can associate the highest (e^-)–(h^+) recombination process observed in the thinner film to the presence of intermediate levels close the conduction band.

The high recombination rate at the surface and grain boundary, provoked by high level of surface states, is another plausible hypothesis to explain the low photocurrent reported for the thinner film.[9] However this hypothesis has little likelihood because both films (the thicker and the thinner films) presented a similar grain size and the same Si concentration.

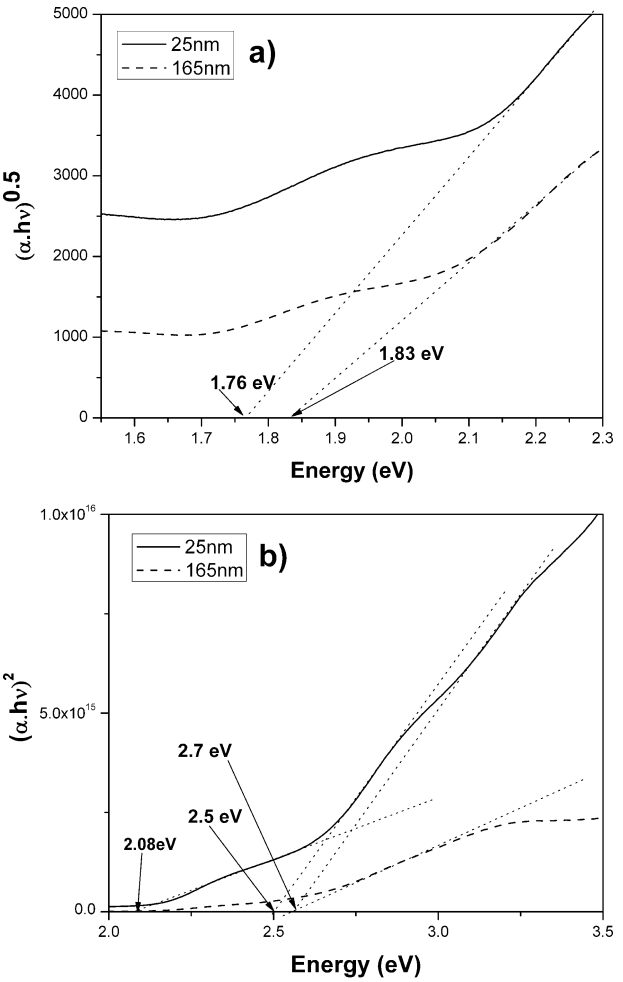

Fig. 6 Plot of absorption data according to eqn (1): (a) indirect band gap; (b) direct band gap.

Conclusions

In summary, the results presented here show that the optical property of the hematite film is strongly affected by film thickness, probably due to the stress induced by the strong interaction between film and substrate. This stress generates defects in the crystal lattice of the hematite film, increasing the (e^-)–(h^+) recombination process. Several theoretical and experimental works in the literature show that a distortion in the lattice structure can generate distortion in the electronic structure,[15,16] hence supporting our argument. This result is interesting because it can propose a new explanation for the improvement of the photocurrent when a very thin layer is deposited between the hematite film and the substrate.[8,12] In fact, this layer can decrease the stress generated in the film/substrate interface, resulting in a film with low defect concentration.

Acknowledgements

The authors would like to gratefully acknowledge the Brazilian funding agencies FAPESP/CEPID (project 98/14324-0) and CNPq.

References

1 A. Fujishima and K. Honda, *Nature*, 1972, **238**, 37.
2 J. H. Park, S. Kim and A. J. Bard, *Nano Lett.*, 2006, **6**, 24–28.
3 M. Matsuoka, M. Kitano, M. Takeuchi, K. Tsujimaru, M. Anpo and J. M. Thomas, *Catal. Today*, 2007, **122**, 51–61.
4 K. G. Mor, H. E. Prakasam, O. K. Varghese, K. Shankar and C. A. Grimes, *Nano Lett.*, 2007, **7**(8), 2356–2364.
5 A. B. Murphy, P. R. F. Barnes, L. K. Randeniya, I. C. Plumb, I. E. Grey, M. D. Horne and J. A. Glasscock, *Int. J. Hydrogen Energy*, 2006, **31**, 1999–2017.

6 A. Duret and M. Gratzel, *J. Phys. Chem. B*, 2005, **109**, 17184–17191.
7 I. Cesar, A. Kay, J. A. Gonzalez Martinez and M. Gratzel, *J. Am. Chem. Soc*., 2006, **128**(14), 4582–4583.
8 A. Kay, I. Cesar and M. Gratzel, *J. Am. Chem. Soc*., 2006, **128**(49), 15714–15721.
9 J. A. Glasscock, P. R. F. Barnes, I. C. Plumb and N. Savvides, *J. Phys. Chem. C*, 2007, **111**, 16477–16488.
10 M. P. Dare-Edwards, J. P. Goodnough, A. Hamnett and P. R. Trevellick, *J. Chem. Soc., Faraday Trans*., 1983, **79**, 2027–2041.
11 J. H. Kennedy and K. W. Frese, Jr, *J. Electrochem. Soc*., 1978, **125**(5), 709–714.
12 R. van de Krol, Y. Liang and J. Schoonman, *J. Mater. Chem*., 2008, **18**, 2311–2320.
13 (*a*) V. Bouquet, M. I. B. Bernardi, S. M. Zanetti, E. R. Leite, E. Longo, J. A. Varela, M. G. Viry and A. Perrin, *J. Mater. Res*., 2000, **15**, 2446; (*b*) F. M. Pontes, E. R. Leite, G. P. Mambrini, M. T. Escote, E. Longo and J. A. Varela, *Appl. Phys. Lett*., 2004, **84**, 248; (*c*) G. P. Mambrini, E. R. Leite, M. T. Escote, A. J. Chiquito, E. Longo, J. A. Varela and R. F. Jardim, *J. Appl. Phys*., 2007, **102**, 043708.
14 J. I. Pankor, *Optical processes in semiconductors*, Prentice Hall, New Jersey, 1971.
15 E. Orhan, J. A. Varela, A. Zenatti, M. F. C. Gurgel, F. M. Pontes, E. R. Leite, E. Longo, P. S. Pizani, A. Beltran and J. Andres, *Phys. Rev. B*, 2005, **71**, 085113.
16 N. Pailhé, A. Wattiaux, M. Gaudon and A. Demourgues, *J. Solid State Chem*., 2008, **181**, 1040–1047.